J. Fluid Mech. (2007), *vol.* 584, *pp.* 337–356.
doi:10.1017/S0022112007006374 Printed in the United Kingdom

Mass flow rate measurements in a microchannel, from hydrodynamic to near free molecular regimes

TIMOTHÉE EWART, PIERRE PERRIER, IRINA A. GRAUR AND J. GILBERT MÉOLANS

Université de Provence – Ecole Polytechnique Universitaire de Marseille,
Département de Mécanique Energétique – UMR CNRS 6595,
5 rue Enrico Fermi, 13453 Marseille cedex 13, France
timothee.ewart@polytech.univ-mrs.fr

(Received 18 July 2006 and in revised form 10 March 2007)

Helium mass flow rates in a microchannel were measured, for a wide Knudsen-number range, in isothermal steady conditions. The flow Knudsen numbers, considered here, cover the range from continuum slip regime to the near free molecular regime. We used a single-channel system involved in an experimental platform more powerful than those previously used. The experimental errors and uncertainties were accurately investigated and estimated. In the continuum slip regime, it was found that the first-order approach is pertinent for Knudsen number between 0.03 and 0.3. Moreover, the slip coefficient was deduced by comparing the experiments with the theoretical first-order slip continuum approach. For Knudsen number between 0.03 and 0.7, a polynomial second-power form is proposed for the mass flow rate expression. Otherwise, the experimental results on the mass flow rate were compared with theoretical values calculated from kinetic approaches over the 0.03–50 Knudsen number range, and an overall agreement appears through the comparison. It was also found, when the Knudsen number increased, that the wall influence on measurement occurred first through the accommodation process in the transition regime followed by the wall influence through the aspect ratio in the free molecular regime.

1. Introduction

The development of microelectromechanical systems (MEMS) requires correct prediction of the rarefied flows occurring in many kinds of small devices, such as micro-pumps and micro-sensors. The necessity of optimizing their designs has opened new prospects in the domain of rarefied gas experiments. MEMS appeared in the early 1980s, and since then many papers on gas microflows have been published. These studies concentrated on channel geometry and were limited to slip and near transitional regimes (Pong *et al.* 1994; Harley *et al.* 1995; Arkilic *et al.* 1997, 2001; Zohar *et al.* 2002; Maurer *et al.* 2003; Colin, Lalonde & Caen 2004).

In the present work, we extend the mass flow rate measurements for gas microflows ranging from the continuum to the near free molecular regime, based on a single microchannel. For such a geometry and for such a wide range of flow regimes, very few measurements have been carried out: over the last fifty years, only one experimental series involving different microchannels has been presented (Porodnov *et al.* 1974), whereas many measurements have been carried out for the tube geometry

from the continuum to the free molecular regime (Dong 1956; Porodnov *et al.* 1974; Tison 1993). The present measurements involve two main original features (especially when compared to the measurements performed by Porodnov *et al.* 1974): first, our experiments are carried out for inlet/outlet pressure ratios ranging between 3 and 5, i.e. for non-dimensional pressure gradients of the same order as the pressure itself, whereas in the Porodnov *et al.* (1974) experiments, the relative inlet/outlet pressure difference is smaller than 1 %; secondly, the Porodnov *et al.* (1974) measurement method is an unsteady procedure giving the gas volume flow rate whereas we use a new measurement technique (Ewart *et al.* 2006) which allows us to measure very low mass flow rates ($<10^{-12}\,\mathrm{kg\,s^{-1}}$) using a sensitive pressure gauge in order to detect very small pressure rises in the outlet tank. The lack of results concerning the free molecular regime in microchannels can be explained by the difficulties encountered so far in accurately measuring such low mass flow rates.

The purpose of the present study is two-fold: (i) completing the database of mass flow rate measurements, obtained in a single microchannel, ranging from the continuum slip regime to the near free molecular regime; (ii) exploring the properties of the gas/surface interaction according to the different flow regimes investigated here and also according to various pressure gradient mean values. Therefore, in the slip regime, the measured data of mass flow rates are compared with the analytical solution of the Navier–Stokes equations associated to the first-order boundary condition. The 'experimental' velocity slip coefficient and the tangential momentum accommodation coefficient (TMAC) are derived using this type of boundary condition and the pertinence of a Knudsen number first-order treatment for helium is shown in the 0.03–0.3 Knudsen number range. In the transition regime and in the near free molecular regime, the measured data are compared with the theoretical results deduced from the Boltzmann equation using various models: the BGK model (Loyalka 1975; Loyalka, Stvorik & Park 1976) or the S model (Sharipov 1999*a*). The theoretical results obtained by solving the linearized Boltzmann equation (Ohwada, Sone & Aoki 1989; Hickey & Loyalka 1990) were also considered for comparison. Globally, our measurements appear in good agreement with the theoretical results. Nevertheless, the full diffuse reflection at the wall, largely assumed in the theoretical kinetic approaches, does not yield satisfactory fitting between the theoretical results and the experimental mass flow rate values. Thus, the diffuse specular model (according to a Maxwell-type reflection law) seems more suitable for describing the gas/wall interaction. However, the tangential momentum accommodation coefficients deduced using this theoretical frame turn out to be different in the slip regime and in the near free molecular regime. Further investigations and complementary analyses are necessary to confirm this conclusion.

2. Experiments

2.1. *Description of the methodology and experimental set-up*

The experimental method used in the present work to measure the mass flow rate through a microchannel involves the use of two constant volume tanks and so may be denoted a 'constant-volume technique'. This method requires very large tank volumes, much larger than the volume of the microchannel. Large tank sizes guarantee that the microflow parameters are independent of time: although detectible, the mass variations occurring in the tanks during the experiments do not call into question the steady assumption. Thus, we must also set a limit for the maximal suitable variation of the pressure in the second tank, according to the inlet and outlet conditions. These

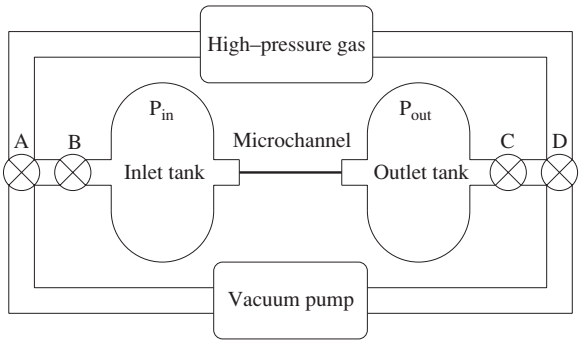

FIGURE 1. Mass flow experiment diagram. The valves A to D are used to impose and to adjust the pressure in the inlet and outlet tanks.

Detectors	A	B	C	D
Full scale FS (Pa)	133 322	13 332.2	1333.22	133.322
Pressure limit max (Pa)	133 322	13 332.2	1333.22	133.322
Pressure limit min (Pa)	13 332	1333.2	133.32	13.332
Accuracy	0.20 % of reading			
Temperature effect on zero	0.0050 % FS/K			0.015 % FS/K
Temperature effect on span	0.01 % of reading/K			
Resolution	0.0015 % FS			0.0025 % FS
Inficon CDG	25-1000 T	25-100 T	25-10 T	45-1 T

TABLE 1. Technical data for the gas detectors manufactured by Inficon. The four detectors have similar characteristics, but their full scales are different.

constraints are taken into account in the experimental set-up (figure 1). The gas flows through a silicon microchannel fixed between two tanks in which the pressures remain very close to the constant values P_{in} and P_{out}, respectively. The pressure variation in the second tank owing to the gas flow through the microchannel is set at ± 1 % of the tank pressure averaged over the experiment. Consequently, the relative pressure variation in the first tank remains close to the $\pm$(0.2 %–0.33 %) depending on the pressure ratio between the tanks. This pressure variation range corresponds to a required experiment duration τ ranging from about a few seconds for the highest mass flow rate measured (10^{-9} kg s^{-1}) to about 120 s for the lowest (10^{-13} kg s^{-1}).

The pressure measurements are carried out using simultaneously two detectors chosen according to the pressure range (see table 1). One is located in the first tank upstream of the microchannel and the other in the second tank downstream of the microchannel. The errors in pressure measurements in each tank depend on the characteristics of the pressure detectors (table 1). Thus, in the pressure range observed during the experiments, the errors on the measurement of the outlet pressures may be estimated to be smaller than 0.5 %.

It is also very important to measure the dimensions of the channel accurately because the geometrical characteristics have a great influence on the mass flow rate: for example, the analytical expression of the mass flow rate, in hydrodynamic and slip regimes, is proportional to the power three of the channel height. Therefore, the surfaces of the inlet and outlet sections have been scanned in the environmental scanning mode (ESEM) with an electron microscope and the following estimations

of the channel dimensions have been obtained: the channel height H is $9.38 \pm 0.2\,\mu m$, its width w is $492 \pm 1\,\mu m$ and its length L is $9.39 \pm 0.1\,mm$. Since the length of the channel is much greater than its height, the channel end effects can be neglected. Moreover, the roughness of the channel walls is estimated to be smaller than 20 nm.

The details about the connections required in the gas circuit and the estimation of the leakage may be found in Ewart *et al.* (2006). The experiments are performed within a narrow temperature range, excluding any heat source in the environment. During each experiment, the temperature is not maintained, but controlled to be sufficiently constant to justify the isothermal assumption as quantified in the following section.

2.2. *Analysis of the non-isothermal effects*

The technique used to measure the mass flow rate consists in determining in the outlet tank a small pressure change due to the mass flowing from the microchannel. The temperature variation in the outlet tank could directly perturb the significance of the measurement. To make this clearer, let us write for this tank the law of perfect gases in the form:

$$P_{out} V = m \mathscr{R} T, \tag{2.1}$$

where V represents the outlet tank volume which remains constant during the experiment, and $\mathscr{R}$ is the specific gas constant. P_{out}, T and m are, respectively, the pressure, temperature and mass of the gas in the outlet tank, at any time t of the experiment time length τ. Let us define the variation $\mathrm{d}q$ of any thermodynamic parameter q, occurring in the tank during the experiment time length (whatever the reason for these variations). According to the comments made in the previous section, these relative variations remain small, compared to 1. Therefore, they are deduced from (2.1), verifying the relation

$$\frac{\mathrm{d}P_{out}}{P_{out}} = \frac{\mathrm{d}m}{m} + \frac{\mathrm{d}T}{T}, \tag{2.2}$$

which is easily transformed into:

$$\frac{\mathrm{d}m}{\tau} = \frac{V}{RT}\frac{\mathrm{d}P_{out}}{\tau}(1-\varepsilon), \qquad \varepsilon = \frac{\mathrm{d}T/T}{\mathrm{d}P_{out}/P_{out}}. \tag{2.3}$$

If ε is very small compared to 1, then $\mathrm{d}m/\tau$ may be identified as the mass flow rate Q_m flowing from the microchannel, and $\mathrm{d}P_{out}$ (termed δP_{out} below) will allow direct measurements of Q_m. The maximal instantaneous temperature departure (from its initial value) registered during the experiments is smaller than half a degree. Such a departure certainly overestimates the probable temperature variation at any time. Therefore, from the various points acquired during the experimental time τ, we calculate the mean temperature value $\overline{T}$ and its corresponding standard deviation s. The specification of the standard deviation is influenced (and so overestimated) by the noise of the temperature probe and electronic acquisition card. Nevertheless, in the present experiment, this estimation appears as a pertinent evaluation of the probable temperature variation. In the most unfavourable case, this estimation leads to a relative variation $\delta T/T = s/T$ around the mean temperature equal to 0.0002, lower than 0.01 for the relative variation $\delta P_{out}/P_{out}$: ε is clearly smaller than 0.02. Thus, the measurement based on the pressure rise may be considered as the measurement of an isothermal mass flow rate,

$$Q_m = \frac{V}{\mathscr{R}T}\frac{\delta P_{out}}{\tau}, \tag{2.4}$$

affected by a specific relative error of ± 0.02 due to the temperature variations (see (2.6)).

2.3. *Pressure rise measurements and experimental error*

Since the effects of the temperature variation are negligible, we may consider the flow through the microchannel as a steady flow occurring between two tanks maintained at pressures P_{in} and P_{out}, practically constant, respectively, with variations of the order of $\pm 1\,\%$ in the outlet tank and of the order of $\pm(0.2\,\%–0.33\,\%)$ in the inlet tank (see § 2.1). These variations are smaller than the experimental error, and are consistent with the steady assumption. Moreover, the isothermal mass flow rate may be expressed in the form (2.4). To determine this mass flow rate, we will use the registered data for pressures P_i at time instants t_i. The stationary flow conditions physically justify a pressure rise interpolation by means of a linear function of time using a simple least-squares fit

$$P_f(t) = at + b, \qquad a = \frac{\delta P_{out}}{\tau}. \tag{2.5}$$

The calculation of the coefficient a is characterized by a convenient value of the usual determination coefficient r^2, greater than 0.9993. Under the reasonable assumption of negligible errors in determining the fixed time values t_i, the error on coefficient a is calculated using the classical expression of the errors on the linear fitting coefficients of the least-squares method and yields a relative error smaller than $\pm 0.1\,\%$, in all the cases where the error calculation is fulfilled; then to increase the reliability of this evaluation we adopt a large upper bound of this error value ($\pm 0.5\,\%$). Thus, the usual evaluation of the measurement errors results from (2.4), (2.5) as:

$$\frac{\Delta Q_m}{Q_m} = \frac{\Delta V}{V} + \frac{\Delta T}{T} + \frac{\Delta a}{a}, \tag{2.6}$$

where $\Delta T/T$, obtained through the temperature measurements, is negligible, but where the non-isothermal effects previously evaluated ($\pm 2\,\%$) must be taken into account in the evaluation of $\Delta Q_m/Q_m$. $\Delta V/V$ is the uncertainty on the volume measurement ($\pm 2\,\%$) and $\Delta a/a$ is the error on coefficient a ($\pm 0.5\,\%$ as seen above). Moreover, since the leaks are estimated as totally negligible (Ewart *et al.* 2006), we do not integrate them in the total uncertainty on the mass flow rate. Therefore, we obtain a full uncertainty on $\Delta Q_m/Q_m$ smaller than $\pm 4.5\,\%$. The capabilities of the sensors and vacuum pump employed so far did not allow us to reach the full free molecular regime. Using the more powerful equipment now available will make it possible to extend the investigations up to Knudsen numbers about five times higher.

3. Background theory

The flow in a rectangular channel has been studied experimentally for Knudsen numbers ranging from 0.03 to 50, which means that the observed flow regime changes from the hydrodynamic to the near free molecular regime. Many different theoretical and numerical approaches have been used to solve the problem of gas flow through a long channel (or two parallel plates) under isothermal flow conditions for a wide Knudsen-number range (see Sharipov & Seleznev 1998; Karniadakis & Beskok 2002; Graur, Méolans & Zeitoun 2006). We will present briefly the theoretical approaches used in order to compare the measured and theoretical values of the mass flow rate and of the velocity slip coefficients.

3.1. *Hydrodynamic and slip regimes*

In the hydrodynamic and slip regimes, the flow through a rectangular channel has been intensively studied and the problem of the choice of the appropriate boundary conditions (first- or second-order following the Knudsen number) and the problem of the limit of validity of the continuum approach (in terms of the Knudsen-number range) remain an open question. In hydrodynamic and slip flow regimes, the flow analysis may be developed using the continuum macroscopic equations (Navier–Stokes equations) supplemented with slip boundary conditions at the wall. Assuming a possible second-order boundary condition at the wall, in the isothermal case the slip velocity reads:

$$u_s = \pm A_1 \lambda \left(\frac{\partial u}{\partial y}\right)_w - A_2 \lambda^2 \left(\frac{\partial^2 u}{\partial y^2}\right)_w, \tag{3.1}$$

where λ is the mean free path of the molecules which may be calculated using the following well-known expression, very similar to that of the hard-sphere (HS) model (Chapman & Cowling 1970)

$$\lambda = k_\lambda \frac{\mu}{P}\sqrt{2\mathscr{R}T}, \qquad k_\lambda = \frac{\sqrt{\pi}}{2}. \tag{3.2}$$

In the physical conditions of the present study, we can use only the first-order boundary condition, so the coefficient $A_2 = 0$ and the slip condition (3.1) reads:

$$u_s = \pm A_1 \lambda \left(\frac{\partial u}{\partial y}\right)_w. \tag{3.3}$$

In this theoretical frame, the coefficient A_1 may be presented in the form:

$$A_1 = \frac{\sigma_p}{k_\lambda}, \tag{3.4}$$

where σ_p is the velocity slip coefficient. The mass flow rate through the rectangular channel obtained from the Navier–Stokes equations with the first-order velocity slip condition (Graur *et al.* 2006) is:

$$\dot{M} = \frac{H^3 w \Delta P P_m}{12\mu\mathscr{R}TL}(1 + 6A_1 Kn_m), \tag{3.5}$$

where $\Delta P = P_{in} - P_{out}$, $\mathscr{P} = P_{in}/P_{out}$ and $Kn_m = \lambda/H$ is the mean Knudsen number, based on the mean pressure $P_m = 0.5(P_{in} + P_{out})$. This mean pressure is used in (3.2) in order to determine the averaged mean free path. The influence of the lateral walls on the mass flow rate is not taken into account, which is a correct approximation when $H \ll w$, as is the case here. According to Sharipov (1999*a*) the lateral wall influence may be taken into account by the factor $1 - 0.63H/w$ multiplying the mass flow rate $\dot{M}$, which gives 0.99 in our case where $H/w = 0.019$.

Furthermore, a non-dimensional mass flow rate may be deduced from (3.5):

$$S = \dot{M} \Big/ \frac{H^3 w \Delta P P_m}{12\mu\mathscr{R}TL} = 1 + 6A_1 Kn_m. \tag{3.6}$$

Equation (3.6) may be rewritten in the more compact form:

$$S = 1 + A^{theor} Kn_m, \tag{3.7}$$

where $A^{theor} = 6A_1$. The analytical expressions of the mass flow rate (3.5)–(3.7) will be used for the calculation and the comparison with the corresponding measured

values. We use the measured values of the mass flow rate for two main purposes: to obtain the 'experimental' velocity slip coefficient; and to establish the limit of the applicability of the continuum equations for this kind of flow. The term σ_p appears to depend on the gas interaction model only through the viscosity μ.

3.2. *Free molecular regime*

In the case of a free molecular regime, the mass flow rate between two parallel plates was obtained analytically by Cercignani & Daneri (1963) under the assumption of full accommodation of the molecules at the wall and by Sharipov & Seleznev (1998) in the case of the diffuse-specular scattering at the wall. For a channel of finite width, the mass flow rate of the free molecular regime was found by Loyalka *et al.* (1976) for a diffuse reflection of the molecules from the wall. In the case of two parallel plates, the dimensionless mass flow rate, reduced as usual in the transitional regime, tends to infinity when the Knudsen number increases (Cercignani & Daneri 1963). This may be partly due to the characteristic mass flow rate chosen to define the non-dimensional flow rate (see § 3.3); but whatever the choice, the influence of the section aspect ratio will increase when the Knudsen number increases because then the gas/gas collisions vanish and only the gas/wall collisions govern the flow behaviour. Therefore in § 4, we will see that the models involving two parallel plates differ more and more from our experimental results when Kn increases strongly.

3.3. *Transition flow regime*

The most complicated domain for modelling is the transition flow regime, where the Boltzmann equation should be solved. A review of the main results obtained in this field may be found in Sharipov & Seleznev (1998). We will detail only the results which are the most useful for the analysis of our experimental measurements. We will start with the modelling of the flow between two parallel plates. The expression of a volume flow rate between two parallel plates, for a large Knudsen-number range, was obtained by Cercignani & Daneri (1963) solving the BGK kinetic equation by the discrete ordinate method and assuming a diffuse reflection of the molecules from the wall. The BGK model again, this time associated with a diffuse-specular reflection on the solid surface, was also considered by Loyalka (1975). Moreover, the linearized Boltzmann equation for the flow between two parallel plates was solved by Ohwada *et al.* (1989) and Hickey & Loyalka (1990) for hard-sphere molecules and for a diffuse reflection as boundary condition. The difference between the solution of the BGK equation and that of the Boltzmann equation is only about 2 % (Sharipov & Seleznev 1998). The finite dimensions of the rectangular channel were taken into account by Loyalka *et al.* (1976) when solving numerically the BGK kinetic equation using a diffuse scattering. In this same case of rectangular channels with arbitrary height to width ratios, two modellings of the collision integral: the BGK-model (Sharipov 1999*a*) and the S-model (Sharipov 1999*b*), both assuming a complete accommodation of the molecules on the wall, were compared. In the isothermal case, the difference between the mass flow rates obtained with these two models is less than 1 % (Sharipov & Seleznev 1998). Since, as seen above, the difference between the solution of the linearized Boltzmann equation and those of the two kinetic equation models is also small, we will use below only the results given by the solution of the BGK model (Sharipov 1999*a*) and (Loyalka 1975) in order to compare the theoretical results with our measurements.

All the approaches presented above use the same basic assumption: the local pressure gradient, defined as follows, is small:

$$\nu = \frac{H}{P}\frac{\mathrm{d}P}{\mathrm{d}x} \ll 1. \tag{3.8}$$

According to many authors (quoted above) this assumption allows the linearization of the kinetic equation and that of the boundary conditions around an equilibrium state, and so the calculation of a dimensionless flow rate Q through a cross-section of the channel (or through a standard width, in the case of two infinite plates). This dimensionless mass flow rate is

$$Q = -\frac{\sqrt{2\mathscr{R}T}}{Hw\,P\nu}\dot{M}, \tag{3.9}$$

when the local pressure gradient $\mathrm{d}P/\mathrm{d}x$ does not vary too much along the channel, (3.9) does not vary either. Moreover, in this case, the dimensionless flow rate is roughly independent of the mean pressure gradient characterizing the flow, but it depends mainly on its rarefaction parameter (i.e. on an inverse Knudsen number):

$$\delta = \frac{\sqrt{\pi}}{2}\frac{H}{\lambda}. \tag{3.10}$$

This non-dimensional mass flow rate (3.9) considered as a function of the local rarefaction parameter (3.10) was calculated by many authors (Loyalka 1975; Loyalka *et al.* 1976; Ohwada *et al.* 1989; Hickey & Loyalka 1990; Sharipov 1999*a*, *b*). In all these theoretical papers, the rarefaction parameter δ is supposed practically constant along the channel. This assumption seems to be much more restrictive than (3.8). However, in our experimental measurements, the pressure variations along the channel are considerable (the ratio between the pressures in the inlet and outlet tanks ranges between 3 and 5), and so the pressure ratios are very high compared to 1 and the rarefaction parameter is not constant along the channel. However, some authors (Sharipov & Seleznev 1998), consider that in a long channel, the local pressure gradient defined as in (3.8) is always small at any pressure ratio, then it is possible to apply this theoretical approach in the case of high pressure ratios, but it is necessary to take into account the changes in the rarefaction parameter owing to the pressure changes that are not small.

In order to compare our experimental results with existing theoretical models, we adopted this point of view; i.e. we consider our theoretical results obtained in different flows as being obtained in the same flow at different locations of the channel and so for different local values of the rarefaction parameter. Nevertheless, in practice, it is difficult to compare the measured and the calculated mass flow rates using the dimensionless form (3.9), as the local pressure and local rarefaction parameter are unknown. Therefore, integrating the two members of (3.9) along the channel and using the property of the mass flow rate conservation, we deduce the following:

$$G = \frac{L\sqrt{2\mathscr{R}T}}{H^2 w(P_{in} - P_{out})}\dot{M}, \tag{3.11}$$

with

$$G(\delta_{in}, \delta_{out}) = \frac{1}{\delta_{out} - \delta_{in}}\int_{\delta_{in}}^{\delta_{out}} Q(\delta)\,\mathrm{d}\delta. \tag{3.12}$$

As noted in Sharipov (1999*a*), G, which is the mean value of Q along the channel, no longer depends on the local pressure gradient, but only on its mean value.

$\mathscr{P}$	5		4		3	
Quantity	*Min*	*Max*	*Min*	*Max*	*Min*	*Max*
Mass flow rate (10^{-13} kg s^{-1})	4.94	21 100	5.29	22 500	8.16	15 100
Inlet pressure (Pa)	60.4	109 825	65.1	115 474	121.2	96 665
Outlet pressure (Pa)	12.2	22 633	15.9	29 275	40.3	32 654
Average Knudsen number Kn_m	0.027	50.2	0.025	45.4	0.028	22.76
Experiment $\mathscr{P}_E$	4.82	5.14	3.90	4.11	2.90	3.06
Centred $\mathscr{P}_C$	4.98		4.01		2.98	

TABLE 2. Experimental pressure range. $\mathscr{P}$ represents the desired ratio P_{in}/P_{out}, whereas $\mathscr{P}_E$ is the real ratio for each measurement, $\mathscr{P}_C$ is the mean experimental ratio of $\mathscr{P}_E$.

The equations (3.11) and (3.12) may be used to calculate numerically the reduced mass flow rate $G(\delta_{in}, \delta_{out})$ from the table of $Q(\delta)$ in Sharipov (1999*a*), where this non-dimensional mass flow rate Q has been obtained from the BGK kinetic equation for rectangular channels with various aspect ratios. In order to analyse the influence of the gas/wall interaction on the mass flow rate, we will also use these relations to compare our experimental data to the reduced mass flow rate obtained from the BGK model kinetic equation used with a diffuse-specular scattering in Loyalka (1975): he considers the flow between two parallel plates and we compare the measured and theoretical values of the mass flow rate per width unit. A solution of the BGK equation also with a diffuse-specular scattering is presented in Loyalka *et al.* (1976) for a channel of finite rectangular section with an aspect ratio of 1, which unfortunately is different from the very small ratio used in our experiments.

4. Results and discussion

The helium flow is studied for different flow regimes: from the hydrodynamic regime for which the mean Knudsen number is 0.03 to the near free molecular regime corresponding to a mean Knudsen number of 50. Each experiment is carried out with a constant pressure ratio $\mathscr{P}$ between the tanks. The real pressure ratios $\mathscr{P}_E$ maintained in each experiment lie within narrow bands centred around three pressure ratios $\mathscr{P}_C$ close to $\mathscr{P} = 3, 4$ and 5, respectively. The properties of these three series are summarized in table 2. The results obtained for $\mathscr{P} = 5$ are detailed in table 3.

The total Knudsen-number range investigated is too wide to be globally analysed using a continuum approach. Therefore, we split the total Knudsen number range into several parts and we consider first a part of this range below a maximum Knudsen number of 0.7, relevant to the slip regime and, probably, to the beginning of the transitional regime.

4.1. *Polynomial expressions of the mass flow rate in slip and near transitional regimes*

In this first range, the experimental dimensionless mass flow rate data are fitted with first- and second-power polynomial forms of Kn_m:

$$S_f^{exp} = 1 + A_i^{exp} Kn_m + B_i^{exp} Kn_m^2, \qquad i = 1, 2, \tag{4.1}$$

by using a nonlinear least-squares method (Maurer *et al.* 2003), in order to describe these regimes. Here, i corresponds to the order of the polynomial form (therefore $B_1^{exp} = 0$).

Q_m (kg s^{-1})	P_{in} (Pa)	P_{out} (Pa)	T (°K)	Q_m (kg s^{-1})	P_{in} (Pa)	P_{out} (Pa)	T (°K)
2.11×10^{-9}	109 825	22 633	296.56	5.23×10^{-11}	9691	1962.1	293.45
1.77×10^{-9}	99 285	20 432	296.59	4.89×10^{-11}	9330	1878.0	293.54
1.73×10^{-9}	97 760	19 475	296.59	4.43×10^{-11}	8106	1626.5	293.45
1.62×10^{-9}	94 421	19 057	296.60	3.72×10^{-11}	7383	1468.7	293.53
1.39×10^{-9}	86 676	17 503	296.13	3.40×10^{-11}	6772	1354.9	293.60
1.27×10^{-9}	82 128	16 871	296.79	3.53×10^{-11}	6614.4	1308.49	297.16
1.05×10^{-9}	73 523	14 862	296.00	3.33×10^{-11}	6332.5	1265.41	297.16
9.13×10^{-10}	67 442	13 403	295.93	3.35×10^{-11}	6133.5	1228.23	297.16
8.70×10^{-10}	65 709	13 230.8	295.89	3.17×10^{-11}	5831.2	1184.31	297.15
8.18×10^{-10}	63 360	12 805.9	295.88	2.78×10^{-11}	5398.6	1078.08	297.17
7.57×10^{-10}	60 485	12 345.3	295.82	2.72×10^{-11}	4952.0	989.72	297.16
7.55×10^{-10}	60 632	12 197.3	295.78	2.48×10^{-11}	4588.5	913.48	297.17
6.74×10^{-10}	56 471	11 376.1	295.74	2.40×10^{-11}	4267.3	854.60	297.16
6.36×10^{-10}	54 568	11 164.3	296.84	2.24×10^{-11}	4019.8	788.44	297.15
6.05×10^{-10}	52 949	10 743.3	295.71	1.89×10^{-11}	3404.8	680.68	297.15
5.54×10^{-10}	49 977	10 059.8	295.71	1.66×10^{-11}	3042.5	619.29	297.14
5.05×10^{-10}	47 100	9458.3	295.71	1.65×10^{-11}	2897.3	582.72	297.13
4.33×10^{-10}	42 730	8569.9	296.58	1.35×10^{-11}	2348.9	480.42	297.11
3.91×10^{-10}	39 901	8002.1	296.59	1.04×10^{-11}	1752.6	352.00	297.24
3.46×10^{-10}	36 932	7456.8	296.66	9.74×10^{-12}	1624.7	327.42	297.46
2.91×10^{-10}	32 763	6494.8	296.68	8.97×10^{-12}	1469.1	292.49	297.21
2.64×10^{-10}	30 787	6159.4	296.78	7.64×10^{-12}	1242.8	248.85	297.19
2.47×10^{-10}	29 430	5916.6	296.89	7.24×10^{-12}	1159.6	234.29	297.33
2.14×10^{-10}	26 571	5302.5	296.97	6.14×10^{-12}	996.0	196.85	297.20
1.87×10^{-10}	24 041	4869.7	297.08	5.43×10^{-12}	815.8	166.41	297.21
1.54×10^{-10}	21 421	4328.8	297.14	4.83×10^{-12}	736.4	148.64	297.53
1.49×10^{-10}	21 025	4276.7	297.17	3.53×10^{-12}	534.78	107.070	293.71
1.19×10^{-10}	18 580	3774.7	294.85	2.43×10^{-12}	348.33	71.585	293.71
1.05×10^{-10}	16 914	3456.6	295.01	2.37×10^{-12}	339.24	68.922	295.88
1.01×10^{-10}	15 677	3136.8	295.25	1.90×10^{-12}	261.65	52.635	295.88
8.60×10^{-11}	14 218	2889.5	294.92	1.48×10^{-12}	197.14	39.016	295.81
7.85×10^{-11}	13 194	2662.8	295.24	1.07×10^{-12}	132.13	26.106	293.73
6.97×10^{-11}	11 669	2385.2	295.25	9.47×10^{-13}	127.02	26.342	296.45
7.13×10^{-11}	11 595	2337.7	295.05	7.66×10^{-13}	90.62	17.626	295.69
5.62×10^{-11}	10 456	2101.3	295.01	6.62×10^{-13}	82.95	16.850	296.25
5.67×10^{-11}	10 065	2052.8	294.74	5.59×10^{-13}	68.32	13.642	295.65
5.67×10^{-11}	9819	1988.5	294.88	4.94×10^{-13}	60.39	12.208	295.41
5.00×10^{-11}	9548	1912.7	294.75				

TABLE 3. Parameters and results characterizing the experiment conditions for $\mathscr{P} = 5$.

The coefficients A_i^{exp} and B_i^{exp}, obtained by applying the nonlinear least-squares Marquard–Levenberg algorithm to the measured values of the mass flow rate, normalized according to (3.6), are given in table 4. The uncertainty on these coefficients is estimated using the standard error.

As is well known, a second-order effect according to the Knudsen number generally exists in the slip regime and increases when the Knudsen number increases (below one). In order to investigate this question, we compared the pertinence of various fittings, using the linear polynomial form and then the quadratic form defined in (4.1). These comparisons were fulfilled for various partial Knudsen-number ranges and required the introduction of two additional parameters: the determination coefficient r^2 (as given in the software Matlab) and the squared residual sum

$\mathscr{P}$	A_1^{exp}	s_{r_1}	r_1^2	A_2^{exp}	B_2^{exp}	s_{r_2}	r_2^2
			Knudsen range (0.03–0.3)				
5	8.30 ± 0.08	0.064	0.991	7.58 ± 0.20	3.418 ± 0.90	0.054	0.994
4	8.27 ± 0.06	0.043	0.996	7.87 ± 0.18	1.897 ± 0.82	0.040	0.998
3	7.73 ± 0.05	0.015	0.998	7.40 ± 0.12	1.526 ± 0.53	0.025	0.999
3–5	8.15 ± 0.05	0.060	0.992	7.67 ± 0.14	2.29 ± 0.62	0.056	0.993
			Knudsen range (0.03–0.7)				
5	8.69 ± 0.09	0.179	0.989	7.35 ± 0.20	2.80 ± 0.39	0.123	0.995
4	8.48 ± 0.05	0.093	0.997	7.95 ± 0.15	1.10 ± 0.29	0.079	0.998
3	8.54 ± 0.14	0.200	0.989	7.18 ± 0.29	2.36 ± 0.48	0.140	0.995
3–5	8.58 ± 0.05	0.163	0.991	7.57 ± 0.13	2.02 ± 0.24	0.126	0.995

TABLE 4. Experimental coefficients A_i^{exp} and B_i^{exp} obtained from the polynomial fitting of the first ($i = 1$) or second ($i = 2$) degree, s_r is the squared residual sum, and r is the determination coefficient.

$s_r = \sqrt{1/(n-p)\sum e_i^2}$ to estimate the quality of the fit; here $e_i = S_i^{exp} - S_{f_i}^{exp}$ is the local difference between the measured and the fitted values, and so represents the local fitting error, n is the number of measurements, p is the number of unknown coefficients in the fitting model. Analysing the values of these two coefficients given in table 4, we find that the determination coefficients r^2 of the first- and second-power fittings are similar when considering the Knudsen-number range 0.03–0.3; but for the widest range under consideration, 0.03–0.7, the determination coefficient of the second-power fitting is closer to 1 than that of the first-power fitting. Moreover, the values of the squared residual sum s_r are similar for the first- and the second-power fitting in the Knudsen-number range 0.03–0.3. However, for the widest Knudsen-number range (0.03–0.7), the values of s_r are always smaller for the second-power fitting. On this basis, in the Knudsen zone 0.03–0.3, the first-power representation gives globally satisfactory results. Thus, in this range, the quadratic fitting is not required in order to obtain a good approximation of the measured values. Moreover, it appears that the measurements are not sufficiently precise to give significant values of the second-power coefficient. On the other hand, considering the uncertainties on the fitting coefficients and the values of the statistical parameters defined above, in the range 0.03–0.7, the second-power shape becomes apparent.

Furthermore, in order to establish the agreement better between the experimental data and the first- and second-power fittings, respectively, we also compared the errors on the measurements (estimated 4.5 %) with the standard error on the fit curves $\sqrt{(1/n)\Sigma e_i^2}/S_m^{exp}$, here S_m^{exp} is the averaged value of the measured values. Then, regarding the 0.03–0.3 Knudsen-number range, the standard error on the first- and second-power fittings gives the same value, 3.5 %. For the 0.03–0.7 Knudsen-number range, only the standard error on the second-power fitting remains equal to 3.5 %, whereas that on the first-power fitting increases and becomes higher than the experimental error. Thus, considering this new criterion, we again find good agreement for the first-power fitting in the 0.03–0.3 Knudsen-number range and a pertinent quadratic fitting for the 0.03–0.7 range.

The experimental results are presented in figure 2 in a non-dimensional form according to the left-hand side of (3.6). The fittings of the first power (dashed line)

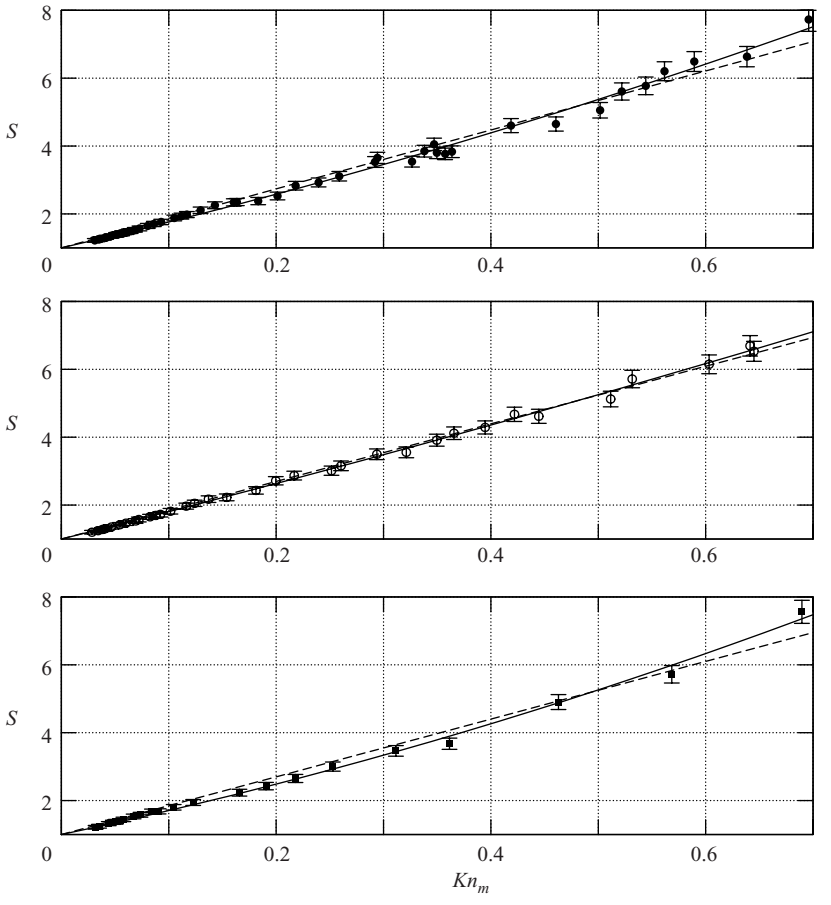

FIGURE 2. Dimensionless mass flow rate obtained according to (3.6). The fitting of the experimental data with the first- (dashed line) and the second- (solid line) power polynomial function. ■, pressure ratio $\mathscr{P} = 3$; ○, 4; ●, 5.

and of the second power (solid line) are also plotted. Figure 2 shows clearly the presence of a slight second-power effect appearing for a mean Knudsen number higher than 0.5, which confirms the analysis given above.

Finally, under the considered conditions (isothermal helium flows in rectangular channels) and in the restricted Knudsen-number range defined above (slip regime and near transitional regime, i.e. $Kn \leqslant 0.7 < 1$), we can again distinguish two regions.

(i) A lower Kn range 0.03–0.3 where the linear fitting appears convenient whereas the quadratic one seems useless and non-significant. Moreover, considering that the corresponding Knudsen values are small enough we have characterized this range as corresponding to hydrodynamic and slip regimes. Thus, we modelled it using the first-order slip continuum model described in § 3.

(ii) A Kn range extending beyond 0.5, and here precisely to 0.7, where, fitting our mass flow rate data, a quadratic behaviour appears clearly according to Kn. Moreover, in this zone, the second-power coefficient becomes significant and largely more precise than all those derived from previous experiments in the same range (Maurer *et al.* 2003).

$\mathscr{P}$	α	σ_p	$\alpha_{1\%}$	$\sigma_{p_{1\%}}$
		Knudsen range (0.03–0.3)		
5	0.900 ± 0.005	1.226 ± 0.011	0.895 ± 0.005	1.238 ± 0.011
4	0.903 ± 0.004	1.221 ± 0.009	0.897 ± 0.004	1.233 ± 0.009
3	0.938 ± 0.004	1.142 ± 0.007	0.933 ± 0.004	1.153 ± 0.007
3–5	0.910 ± 0.004	1.204 ± 0.007	0.905 ± 0.004	1.216 ± 0.007

TABLE 5. Experimental tangential momentum accommodation coefficients (α) and slip coefficients σ_p obtained using the first-power fit. The errors in the table derive from the experimental error in A_1^{exp}. Coefficients $\alpha_{1\%}$, $\sigma_{p_{1\%}}$ are the slip and accommodation coefficients calculated taking into account the correction due to the channel finite-width effects (about 1 %) (Sharipov 1999*a*).

4.1.1. *First-order modelling in the slip regime*

According to the above conclusion, about the Knudsen range 0.03–0.3, we compared theoretical (3.6) and experimental (4.1) mass flow rate expressions. Thus, coefficient A_1 may be expressed in the form:

$$A_1 = \frac{\sigma_p}{k_\lambda} = A_1^{exp}/6. \tag{4.2}$$

This gives the experimental estimation of the velocity slip coefficient summarized in table 5. Of course, this coefficient is calculated using the first-power fitting. This coefficient does not depend significantly on the pressure ratio. These values are slightly different from two theoretical predictions of the slip coefficient: $\sigma_p = 1.012$ given by Kogan (1969) and $\sigma_p = 1.016$ given by Albertoni, Cercignani & Gotusso (1963). These coefficient values have been obtained from the kinetic equation BGK model under the assumption of a full accommodation of the molecules at the wall.

As mentioned in § 3, the value of σ_p is affected by the lateral wall influence (Sharipov 1999*a*). In our case, $H/w = 0.019$, the correction resulting from this influence is about 1 % and we have corrected the value of σ_p in table 5.

Then we compared our results with other experimental results, especially with those concerning the velocity slip measured by Porodnov *et al.* (1974). They assumed a linear dependence of the mass flow rate on the Knudsen-number, which may be justified by the narrow experimental Knudsen-number range (below 0.04) and so they obtained the velocity slip coefficient from volume flow rate measurements using the linear least-squares method. We must take into account that the experimental conditions differ on two other points, which may explain some differences in our respective results. First, the variation of the pressure between the two tanks is much smaller than in our experiments. Moreover, it should be noted that the arrangement of the surfaces for both experimental studies is not the same. Porodnov *et al.* (1974) used a glass surface with two types of irregular roughness: the first one with an averaged value of roughness $\sim$1–5 μm (glass), or, in relative value, 1.1–5.6 % of the channel height; and the second one with an averaged roughness $\sim$0.05 μm (smooth glass), or 0.055 % of their channel height. In the present study, we used a silicon surface with a roughness $\leqslant$20 nm, i.e. in relative value, less then 0.2 % of our channel height, which represents an intermediate value ranging between the roughness of the two types of surface used in Porodnov *et al.* (1974). The value obtained for the slip coefficient is between the two values found by Porodnov *et al.* (1974) (see table 6), which confirms that the roughness is an important characteristic parameter of the surface in our

Coefficient	α	σ_p
Porodnov *et al.* (1974)[2]	0.958 ± 0.005	1.099 ± 0.02
Porodnov *et al.* (1974)[3]	0.862 ± 0.006	1.320 ± 0.01
Colin *et al.* (2004)[1]	0.998	1.02
Maurer *et al.* (2003)[1]	0.977 ± 0.03	1.06 ± 0.07
Present results[1]	0.910 ± 0.003	1.204 ± 0.007
Albertoni *et al.* (1963)[T]	1	1.016

TABLE 6. The tangential momentum accommodation coefficients (α) and the slip coefficient for helium flow ([1]silicon, [2]glass, [3]smooth glass, [T]theoretical values). The accommodation coefficient α is calculated from (4.3). The present results correspond to the 0.03–0.3 Knudsen range and averaged for all the pressure ratios used (line (3–5) in table 5).

measurements, as noted also in Porodnov *et al.* (1974). The nature of the surfaces was also different: glass in Porodnov *et al.* (1974); and silicon in the present work.

Accommodation coefficient. From the experimental estimation of the velocity slip coefficient we also derived the value of the accommodation coefficient using the Maxwell diffuse-scattering model. The use of the usual Maxwell kernel for the gas–surface interaction gives the following value for the velocity slip coefficient, when neglecting the Knudsen-layer influence

$$\sigma_p^M = \frac{\sqrt{\pi}}{2}\frac{2-\alpha}{\alpha},$$

where α is the part of the molecules reflected diffusively. Moreover, it is shown using scattering kernel formalism (Cercignani 1990) that α represents also the accommodation coefficient of any kinetic molecule parameter; but establishing σ_p^M, Maxwell (1878) considered α as the accommodation coefficient of the momentum tangential component, since it is usual to confer this meaning on α when used in the slip coefficient expression.

Nevertheless, in the case of a full accommodation, the theoretical coefficient σ_p^M, which does not include the Knudsen-layer correction, is 0.886, which is different from the well-known theoretical diffuse value given in Albertoni *et al.* (1963). Therefore, we report here another method to calculate the accommodation coefficient proposed by Loyalka, Petrellis & Stvorick (1975) taking into account the Knudsen layer influence. They calculated the values of the slip coefficient using the BGK kinetic model and a Maxwellian diffuse-specular scattering kernel over the whole range of values of accommodation coefficient α; a simple 'modified' expression associating the slip coefficient and the accommodation coefficients was proposed:

$$\sigma_p(\alpha) = \frac{2-\alpha}{\alpha}(\sigma_p(1) - 0.1211(1-\alpha)), \tag{4.3}$$

where $\sigma_p(1)$ is the slip coefficient for $\alpha = 1$ equal to 1.016, i.e. the value theoretically obtained by Albertoni *et al.* (1963).

Thus, based on (4.3) and on the measured value of the velocity slip coefficient, we can calculate the 'experimental' tangential momentum accommodation coefficient α ($\alpha = 0.910$), which is given in table 6 with the accommodation coefficients obtained by other authors. All the measurements quoted in this table were carried out using different experimental techniques, in channels with different surfaces. The results in Colin *et al.* (2004) and Maurer *et al.* (2003) were obtained using the second-power fit

Coefficient	A_2^{exp}	B_2^{exp}	Kn_m
Maurer *et al.* (2003)	7.20 ± 0.3	2.76 ± 1.2	$0.06 - 0.8$
Present results	7.57 ± 0.13	2.02 ± 0.24	$0.03 - 0.7$

TABLE 7. The second-power fitting coefficients A_2^{exp} and B_2^{exp} obtained in Maurer *et al.* (2003) and in the present paper.

and also a larger Knudsen-number range: 0–0.44 in Colin *et al.* (2004) and 0–0.8 in Maurer *et al.* (2003).

We can also estimate the accommodation coefficient using the values obtained numerically, from the BGK kinetic equation in Loyalka (1975), where the mass flow rate is tabulated for a varying coefficient: for our non-dimensional measured values of mass flow rate, using the table given in Loyalka (1975), we find an accommodation coefficient close to 0.96 (within the 0.03–0.3 Knudsen-number range). We give this evaluation process because we shall use this one exclusively for the accommodation evaluation in the transitional and the free regime (see § 4.2). From the previous analysis, we may provisionally conclude that the silicon surface must be described as a quasi-diffuse surface.

4.1.2. *Quadratic mass flow rate behaviour*

The coefficients of the second-power fitting (A_2^{exp}, B_2^{exp}) are given in table 7. The values found for coefficient B_2^{exp} show that a significant Knudsen second-power influence appears when fitting the mass flow rate in the 0.03–0.7 Knudsen-number range. Within this range, we obtained pertinent values for this second-power coefficient. Similar experimental study of this quadratic form was also performed by Maurer *et al.* (2003) and presented as resulting from the second-order effect. These authors processed a large number of measurements obtained for a Kn_m increasing up to 0.8, i.e. in a Knudsen-number range close to our experimental range (0.03–0.7). They reported that their second-order coefficient B_2^{exp} appears very sensitive to experimental errors. In the present work, these errors are much smaller than those in Maurer *et al.* (2003). In any case, as shown in table 7, the results obtained by Maurer *et al.* (2003) are in good agreement with the present results. Considering the respective uncertainties given in table 7, it is clear that the two results are consistent. Of course, this agreement appears as a positive check of our experimental technique. Moreover, this agreement tends to prove that in plan geometry, the second coefficient B_2^{exp} does not depend significantly on the channel height or on the pressure. In addition, the precision, largely better than in Maurer *et al.* (2003), may be improved using new sensors. Thus, this fitting presents some interest for engineering. Nevertheless, even though done by other authors (Maurer *et al.* 2003; Colin *et al.* 2004), we did not analyse this mass flow rate behaviour in the frame of Navier–Stokes second-order modelling, because in our investigations we cannot exclude the possibility that high-order components are involved in the result.

4.2. *Transitional and free molecular regimes*

The measured mass flow rates are given in figure 3 in a non-dimensional form according to (3.11) for pressure ratios $\mathscr{P} = 3$, 4 and 5. The results are plotted as a function of the rarefaction parameter δ_m calculated according to (3.10) using the mean pressure in the channel. The comparison between the results obtained from different pressure ratios sustains the hypothesis that this experimental non-dimensional mass

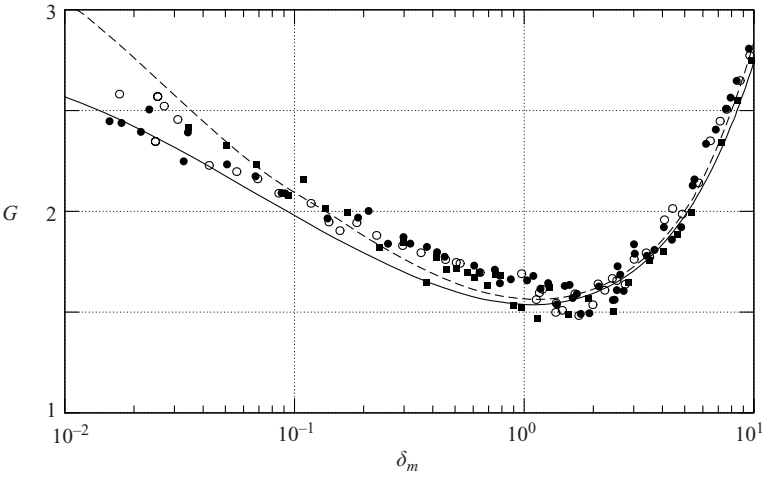

FIGURE 3. Free-molecular scaling of experimental mass flow rate in a channel calculated according to (3.11) with three pressure ratios and theoretical curves: Sharipov (1999*a*) (full line) rectangular channel $H/w = 0.02$ or Loyalka (1975) parallel plates (dash line). ■, pressure ratio $\mathscr{P} = 3$; ○, 4; ●, 5.

flow rate does not depend much on this parameter, as was previously described in the slip regime.

In order to compare this measured mass flow rate with the available theoretical results, we used the numerical solution of the BGK model equation obtained by Sharipov (1999*a*) with a diffuse boundary condition for the molecules impinging on the wall in the rectangular channel with $H/w = 0.02$ cross-section. These results are presented in the form of the non-dimensional mass flow rate Q, (3.9), as a function of δ under the assumption of 'small pressure ratio'. As was mentioned in § 3, we integrated the non-dimensional quantity Q over δ in order to compare with our measurements where the pressure ratio is not close to 1 along the channel. In figure 3, the theoretical mass flow rate obtained after integration (cf. (3.11), (3.12)) is represented as a solid line. In this figure, we also compared our measurements with the results of Loyalka (1975) obtained in the same way for the flows between two parallel plates (dashed line). In the slip regime and at the beginning of the transitional regime, the difference between the mass flow rates from the two theoretical models (parallel plates and channel characterized by a relatively small height/width ratio) is small. However, at the beginning of the free molecular regime ($Kn = 10$–15 or $\delta = 0.07$–0.1), a difference appears between the curves of the two theoretical models. The experimental results apparently behave in a surprising way: in fact, along all the transitional regime and up to the near free molecular regime ($0.7 < Kn < 10$–15, or $1.5 > \delta > 0.1$–0.07) the measurements seem to be rather closer to the theoretical results derived from Loyalka (1975); this probably means that in the transitional regime, the influence of the wall is not yet sufficiently dominant to yield significant differences between the cases $H/w = 0.019$ and $H/w = 0.0$ which corresponds to the theoretical treatment by Loyalka (1975). However, when Kn increases more strongly (δ decreasing strongly) in the full free molecular regime and then when Kn tends to infinity (δ tends to zero) the asymptotic behaviour of the Loyalka (1975) results (parabolic branch) becomes increasingly inappropriate. The measured values (obtained here from $Kn = 15$ up to $Kn = 50$, i.e. $0.01 < \delta < 0.07$) appear increasingly far from the Loyalka solution and close to an asymptotic value predicted by Sharipov (1999*a*).

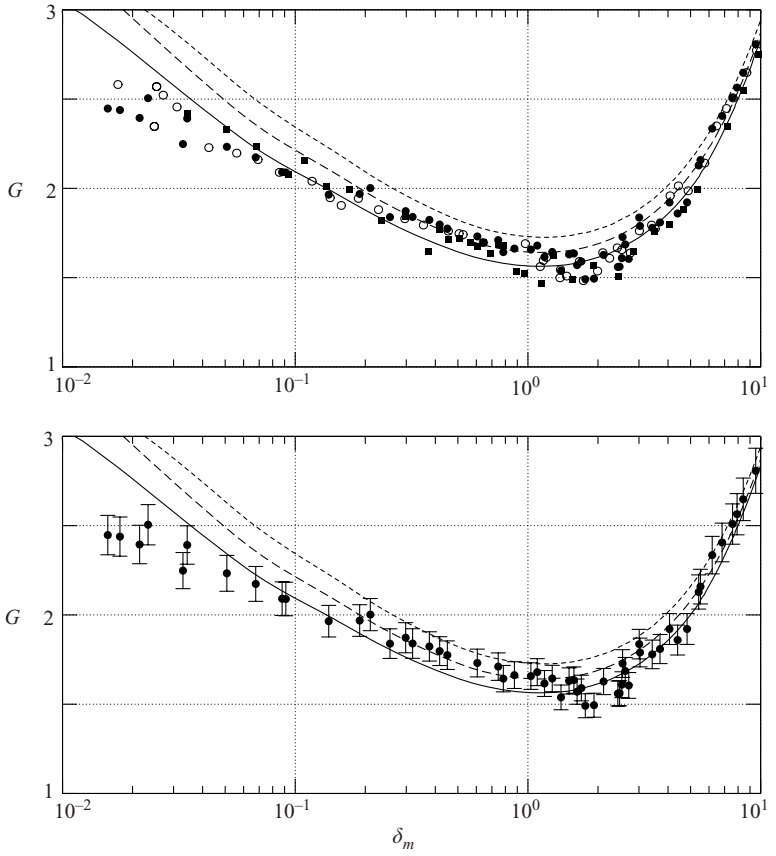

FIGURE 4. Free-molecular scaling of experimental mass flow rate in a channel calculated according to (3.11) with three pressure ratios and theoretical curves (Loyalka 1975) with – – –, $\alpha = 0.92$; - - -, 0.96; —, 1. ■, pressure ratio $\mathscr{P} = 3$; ○, 4; ●, 5.

Furthermore, in order to evaluate now the influence of the surface structure and roughness (rather than that of the surface shape previously analysed through the aspect ratio), we used the results obtained by Loyalka (1975) with the BGK model and the Maxwellian diffuse-specular reflection on the surface. The corresponding non-dimensional mass flow rates G obtained with the technique described above are presented in figure 4 where different values of the accommodation coefficient, ranging from 0.92 to 1, are tested. This study points out two main features: first, in the Knudsen intermediate range defined above ($0.7 < Kn < 10$–15, or $1.5 > \delta > 0.1$–0.07), figure 4 shows that the theoretical model of Loyalka predicts an increasing influence of the accommodation coefficient changes, when the Knudsen number increases. Moreover, according to previous comments on the aspect ratio, in the transitional range, the gas behaves first according to Loyalka (1975) (with $\alpha < 1$) and only then (for a near free molecular regime) does it behave according to Sharipov (1999), where $\alpha = 1$. Thus, it seems that when the rarefaction increases, i.e. when there are relatively more gas/wall collisions than gas/gas collisions, the increase of the boundary-condition effects on the flow operates first through the accommodation phenomenon and only then, through the surface aspect ratio. Secondly, a good agreement of measurements and Loyalka calculations is found for $\alpha = 0.96$, better than for $\alpha = 1$, in the δ range

from 0.1 to 1 (corresponding to the transitional regime). This result confirms that a full accommodation on the surface is inappropriate in the transitional range as well as in the slip regime: moreover, it seems also to indicate, at least in the helium isothermal case, that when the same theoretical frame is applied to analyse experimental results, the same accommodation coefficient (of tangential momentum) is found in the slip and transitional regimes. Globally, the comparison of theory and experiments is satisfactory, if we consider that the experimental measurements are not free from errors and that the finite width of the channel section certainly influences the mass flow rate for very high Knudsen numbers. Therefore, for a more accurate analysis of the combined effects of the partial accommodation and of the non-infinite rectangular section of the channel, it would have been interesting to compare the measurements with theoretical models taking into account both the channel aspect ratio and a diffuse-specular reflection. However, this kind of theoretical result cannot be found in the literature.

5. Conclusions

A technique devoted to the measurement of gas mass flow rates in microchannels is implemented, for isothermal helium flows. A wide Knudsen-number range, from the continuum slip regime to the near free molecular regime, is explored. The errors and uncertainties of the experimental method are accurately investigated and estimated. By analysing the fitting parameters, the pertinence of the first-order velocity slip conditions is shown in the 0.03–0.3 Knudsen range. The accommodation coefficient calculated using the classical Maxwell reflection law associated with the continuum approach, is slightly different (about 5 % smaller) from that deduced from the kinetic approach used by Loyalka (1975). However, both coefficients are smaller than 1, which confirms that the accommodation of helium gas on a silica surface is not completely diffuse. Then, a quadratic form was proposed for the mass flow rate in the 0.03–0.7 Knudsen-number range, possibly useful in engineering.

Then the measured values of the mass flow rate are compared with the corresponding values given by theoretical kinetic approaches over almost all the Knudsen range, especially in the transitional and near free molecular regimes. This comparison is globally satisfactory. The difference between the theoretical curves obtained from the BGK equation for parallel plates and for rectangular channels, respectively, becomes apparent immediately when reaching the transitional regime. However, considering the measurements, the aspect ratio influence becomes significant only from the free molecular regime: then in this regime, even in our case where the aspect ratio of the channel (height/width) is relatively small (0.019), it is necessary to take the lateral wall influence into account.

To deduce the accommodation coefficient in the transitional regime (and possibly in the free molecular regime) only the kinetic method used by Loyalka (1975) (BGK model associated with a Maxwell reflection law) was available. Thus, according to this approach, the influence of the accommodation coefficient (on the mass flow rate) also increases immediately when reaching the transitional regime. Of course, this was not controlled experimentally because it would have required the testing of the helium gas on different surfaces (or at least testing various gases in the same channel) which will be the objective of a future study. Nevertheless, when the Knudsen number increases, the increase of the wall influence on the measurements occurs first (i.e. in the transitional regime) through the accommodation process and then (in the free molecular regime) through the aspect ratio influence. Moreover, using the kinetic

analysis of Loyalka in both transitional and continuum slip regimes we obtain, from experiments, a similar value for the accommodation coefficient, i.e. (as previously seen) a value slightly different from that derived in the slip regime using continuum modelling.

The authors are grateful to the CNRS (National Center of Scientific Research – project number MI2F03-45), the Conseil Régional Provence Alpes Côte d'Azur, the SERES and the RS2N company (Recherche Scientifique et Simulation Numerique, 47 Bd Rabatau, F-13008 Marseille) for their financial support. We should also like to acknowledge Felix Sharipov for valuable discussions.

REFERENCES

Albertoni, S., Cercignani, C. & Gotusso, L. 1963 Numerical evaluation of the slip coefficient. *Phys. Fluids* **6**, 993–996.

Arkilic, E. B., Schmidt, M. A. & Breuer, K. S. 1997 Gaseous slip flow in long microchannels. *J. Microelectromech. syst.* **6**(2), 167–178.

Arkilic, E., Breuer, K. & Schmidt, M. 2001 Mass flow and tangential momentum accommodation in silicon micromachined channels. *J. Fluid Mech.* **437**, 29–43.

Cercignani, C. 1964 Higher order slip according to the linearized Boltzmann equation. Institute of Engineering Res. Rep. AS-64-19, University of California, Berkeley.

Cercignani, C. 1990 *Mathematical Methods in Kinetic Theory*. Plenum.

Cercignani, C. & Daneri, A. 1963 Flow of a rarefied gas between two parallel plates. *Phys. Fluids* **6**, 993–996.

Chapman, S. & Cowling, T. G. 1970 *The Mathematical Theory of Non-uniform Gases*, 3rd edn. Cambridge University Press.

Colin, S., Lalonde, P. & Caen, R. 2004 Validation of a second-order slip flow model in rectangular microchannels. *Heat Transfer Engng* **25**(3), 23–30.

Deissler, R. G. 1964 An analysis of second-order slip flow and temperature-jump boundary conditions for rarefied gases. *Intl J. Heat Mass Transfer* **7**, 681–694.

Dong, W. 1956 Vacuum flow of gases through channels with circular, annular, and rectangular cross sections. *University of California Rep.* UCRL-3353.

Ewart, T., Perrier, P., Graur, I. A. & Meolans, J. G. 2006 Mass flow rate measurements in gas micro flows. *Exps. Fluids* **41**, 487–498.

Graur, I. A., Méolans, J. G. & Zeitoun, D. E. 2006 Analytical and numerical description for isothermal gas flows in microchannels. *Microfluid. Nanofluid.* **2**, 64–77.

Harley, J., Huang, Y., Bau, H. & Zemel, J. 1995 Gas flows in microchannels. *J.Fluid Mech.* **284**, 257–274.

Hickey, K. A. & Loyalka, S. K. 1990 Plane Poiseuille flow: Rigid sphere gas. *J. Vac. Sci. Technol.* A **8**, 957.

Karniadakis, G. E. & Beskok, A. 2002 *Microflows: Fundamentals and Simulation*. Springer.

Kogan, M. N. 1969 *Rarefied Gas Dynamics*. Plenum.

Loyalka, S. K. 1975 Kinetic theory of thermal transpiration and mechanocaloric effects II. *J. Chem. Phys.* **63**, 4054.

Loyalka, S. K., Petrellis, N. & Stvorick, S. T. 1975 Some numerical results for the BGK model: thermal creep and viscous slip problems with arbitrary accommodation of the surface. *Phys. Fluids* **18**, 1094.

Loyalka, S. K., Stvorik, T. S. & Park, H. S. 1976 Poiseulle flow and thermal creep flow in long, rectangular channels in the molecular and transition flow regimes, *J. Vac. Sci. Technol.* **13**, N6, 1188.

Maxwell, J. C. 1878 On stress in rarified gases arising from inequalities of temperature. *Phil. Trans. R. Soc. Lond.* **170**, 231–256.

Maurer, J., Tabelin, P., Joseph, P. & Willaime, H. 2003 Second-order slip laws in microchannels for helium and nitrogen. *Phys. Fluids* **15**, 2613–2621.

Ohwada, T., Sone, Y. & Aoki, K. 1989 Numerical analysis of the Poiseuille and thermal transpiration flows between two parallel plates on the basis of the Boltzmann equation for hard sphere molecules. *Phys. Fluids* A **1**, 2042–2049.

Pong, K., Ho, C., Liu, J. & Tai, Y. 1994 Non-linear pressure distribution in uniform microchannels. In *Application of Microfabrication to Fluid Mechanics ASME, FED* **197**, 51–56.

Porodnov, B. T., Suetin, P. E., Borisov, S. F. & Akinshin, V. D. 1974 Experimental investigation of rarefied gas flow in different channels. *J. Fluid Mech.* **64**, 417–437.

Sharipov, F. 1999*a* Rarefied gas flow through a long rectangular channel. *J. Vac. Sci. Technol.* A **17**, N 5, 3062–3066.

Sharipov, F. 1999*b* Non-isothermal gas flow through rectangular channels. *J. Micromech. Microengng* **9**, 394–401.

Sharipov, F. & Seleznev, V. 1998 Data on internal rarefied gas flows. *J. Phys. Chem. Ref. Data* **27**(3), 657–709.

Suetin, P. E., Porodnov, B. T., Chernjak, V. G. & Borisov, S. F. 1973 Poiseuille flow at arbitrary Knudsen numbers and tangential momentum accommodation. *J. Fluid Mech.* **60**, 585–592.

Tison, S. A. 1993 Experimental data and theoretical modeling of gas flows through metal capillary leaks. *Vacuum* **44**, 1171–1175.

Zohar, Y., Lee, S. Y. K., Lee, W. Y., Jiang, L. & Tong, P. 2002 Subsonic gas flow in a straight and uniform microchannel. *J. Fluid Mech.* **472**, 125–151.